

UC Davis

UC Davis Previously Published Works

Title

Temperatures of Anvil Clouds and Radiative Tropopause in a Wide Array of Cloud-Resolving Simulations

Permalink

<https://escholarship.org/uc/item/1pb3452g>

Journal

Journal of Climate, 35(24)

ISSN

0894-8755

Authors

Seidel, Seth D

Yang, Da

Publication Date

2022-12-15

DOI

10.1175/jcli-d-21-0962.1

Peer reviewed

Temperatures of Anvil Clouds and Radiative Tropopause in a Wide Array of Cloud-Resolving Simulations

SETH D. SEIDEL^{a,b} AND DA YANG^{a,b}

^a *University of California, Davis, Davis, California*

^b *Lawrence Berkeley National Laboratory, Berkeley, California*

(Manuscript received 13 December 2021, in final form 8 August 2022)

ABSTRACT: We present 123 cloud-resolving simulations to study how temperatures of anvil clouds and radiative tropopause (RT) change with surface warming. Our simulation results show that the RT warms at approximately the same rate as anvil clouds. This relationship persists across a variety of modeling choices, including surface temperature, greenhouse gas concentration, and the representation of radiative transfer. We further show that the shifting ozone profile associated with climate warming may give rise to a fixed RT temperature as well as a fixed anvil temperature. This result points to the importance of faithful treatment of ozone in simulating clouds and climate change; the robust anvil–RT relationship may also provide alternative ways to understand what controls anvil temperature.

KEYWORDS: Tropics; Convective clouds; Cirrus clouds; Ozone; Cloud resolving models

1. Introduction

The tropical upper troposphere is home to extensive cirrus clouds detrained from thunderstorms, known as anvil clouds. As the surface warms, anvil clouds are robustly predicted to rise to greater altitudes so that their mean temperature increases less than that of the surface. This holds true in cloud-resolving models (CRMs) (Tompkins and Craig 1999; Kuang and Hartmann 2007; Harrop and Hartmann 2012; Khairoutdinov and Emanuel 2013; Narenpitak et al. 2017) and general circulation models (GCMs) (Zelinka and Hartmann 2010; Thompson et al. 2017), as well as observations (Zelinka and Hartmann 2011). Since anvil clouds' temperature changes little under surface warming, they will emit less longwave radiation to space than if they were to retain the same, warmer altitude. This yields a positive climate feedback when our reference assumption is that clouds would otherwise be fixed in altitude. For this reason, the most recent IPCC report expressed *high confidence* in a positive longwave–cloud altitude feedback (Forster et al. 2021).

The fixed anvil temperature (FAT) hypothesis is the most enduring explanation for the trend of high-cloud temperature with surface warming (Hartmann and Larson 2002). The FAT hypothesis claims that 1) the upper-tropospheric peak in cloud amount is principally the result of the radiatively driven horizontal convergence in clear skies, and 2) this convergence is physically constrained to occur at a fixed temperature where, for fixed relative humidity, the water vapor concentration becomes so small that it loses its ability to efficiently cool the atmosphere. Indeed, studies of CRMs, GCMs, and observations corroborate

the first claim. The upper-tropospheric maximum in convergence covaries with the upper-tropospheric maximum in cloud amount (Kuang and Hartmann 2007; Zelinka and Hartmann 2010; Bony et al. 2016; Seeley et al. 2019b; Zelinka and Hartmann 2011). However, models often contradict the second claim in FAT, showing that anvils and the location of maximum convergence may in fact warm appreciably, albeit slowly compared to the surface. For example, Kuang and Hartmann (Kuang and Hartmann 2007) showed in a CRM that the location of maximum cloud fraction to warm by 2 K when the surface warmed by 8 K, and the recent Radiative-Convective Equilibrium Model Intercomparison Project found an average of 4.4 K of anvil warming over 10 K of surface warming (Wing et al. 2020). This slow but appreciable warming is sometimes known as a Proportionately Higher Anvil Temperature, or PHAT (Zelinka and Hartmann 2010). PHAT is usually found in models where the ozone profile is unrealistically fixed in pressure (Harrop and Hartmann 2012).

It is sometimes assumed that anvil clouds are linked to the radiative tropopause (RT), where radiative heating first goes to zero in the upper troposphere (see, e.g., Birner and Charlesworth 2017; Kluft et al. 2019). The RT is the intersection of the radiative–convective equilibrium (RCE) temperature profile of the troposphere and the radiative or radiative–dynamical equilibrium profile of the stratosphere (Vallis et al. 2015; Hu and Vallis 2019). Since RT is the highest location where latent heating from convection balances radiative cooling in RCE, the RT is also known as the convective top (Thuburn and Craig 2002; Birner and Charlesworth 2017; Dacie et al. 2019). However, convective clouds in fact occur considerably above this point as they overshoot the level of neutral buoyancy (Kuang and Bretherton 2004; Hu et al. 2021). Tompkins and Craig (Tompkins and Craig 1999) found that anvil temperature increased with surface warming in CRM simulations. They suggested this occurred because the RT temperature increases with warming due to their fixed ozone profile. In Kluft et al. (2019), RT is found to warm by about 0.5 K K^{-1} of surface warming in a 1D RCE model without clouds. Assuming a close relationship

Supplemental information related to this paper is available at the Journals Online website: <https://doi.org/10.1175/JCLI-D-21-0962.s1>.

Corresponding authors: Seth Seidel, sdseidel@ucdavis.edu; Da Yang, dayang@ucdavis.edu

between RT and anvil, the authors suggested that their result supported a PHAT. Such an assumption appears to be a crude simplification of FAT/PHAT thinking, according to which a decline in radiative cooling with height below RT causes clear-sky convergence.

Since RT may be simulated by 1D models without clouds, a robust anvil–RT relationship would simplify our understanding of anvil clouds. However, Seeley et al. (Seeley et al. 2019b) achieved a contrary result in “minimal recipe” CRM simulations which isolated the longwave effect of water vapor by removing all other radiative constituents from the model. In their simulations the temperature of RT varied by less than 2 K despite 50 K of surface warming, yet the anvil warming was greater by an order of magnitude. They suggested there is a fixed (radiative) tropopause temperature (FiTT) with respect to surface warming, and RT temperature is unlikely to be related to the temperature of the anvil peak. That is, the top of the troposphere should be disentangled from the anvil location. However, Hartmann et al. (Hartmann et al. 2019) presented CRM simulations in which the anvil, the RT, and a sharp peak in the detrainment of cloud ice each occurred at a fixed temperature despite 5 K of surface warming. They proposed that in convection-permitting RCE simulations the anvil is linked to the location of RT, as convective cooling from overshooting updrafts above the anvil must be compensated by radiative heating. Given this disagreement and the potential clarity provided by an anvil–RT relationship, it is worthwhile to investigate more thoroughly whether the location and temperature anvil clouds are in fact related to the location and temperature of RT.

Modeling choices about ozone are particularly important to the simulated anvil and RT temperatures. Many modeling studies of RCE often use an ozone profile which is unrealistically fixed in pressure, which can give rise to a PHAT (Tompkins and Craig 1999; Kuang and Hartmann 2007; Zelinka and Hartmann 2010; Wing et al. 2020) as well as an increasing RT temperature (Dacie et al. 2019; Kluft et al. 2019). This occurs because the upper troposphere is lifted into a layer of stronger ozone heating. A real atmosphere may give rise to a FAT as climate warming lifts the ozone profile higher in the atmosphere. On this assumption, CRM studies of anvil temperature have modeled an atmosphere with zero ozone (Harrop and Hartmann 2012; Seeley et al. 2019b). In a similar vein, Nowack et al. (Nowack et al. 2015, 2018b) found that prescribing an ozone profile fixed in pressure reduced upper-tropospheric cloud amount in a GCM and reduced the positive cloud–longwave feedback by about $0.1\text{--}0.2\text{ W m}^{-2}\text{ K}^{-1}$ as compared to simulations with interactive ozone. However, those two studies did not isolate the cloud altitude feedback, and to our knowledge it has yet to be explicitly verified whether the upward shift of ozone with warming equally offsets the PHAT behavior to give rise to an approximate FAT.

To test for an anvil–RT relationship, we conduct idealized experiments in a CRM systematically changing the radiation-relevant model settings. We ask: Do changes in model settings that change the simulated RT temperature cause similar changes in the anvil temperature? Are changes in the RT temperature’s *trend* with respect to surface warming associated

with similar changes in the anvil temperature trend? In particular, we test the sensitivity of anvil and RT temperature to the following: 1) a wide range of surface temperatures (280–315 K); 2) the amount of carbon dioxide; 3) the amount of insolation; 4) the shape, concentration, and location of the ozone profile; 5) the presence of a large-scale circulation and convective organization; and 6) the domain size.

2. Simulations

We use the 2D formulation of the System for Atmospheric Modeling (SAM), version 6.10 (Khairoutdinov and Randall 2003). SAM is a cloud-permitting model using the anelastic equations for dynamics. Such 2D CRMs have long been used to study convection and clouds in the tropics (Held et al. 1993; Grabowski et al. 2000; Blossey et al. 2010; Yang 2018a,b; Seidel and Yang 2020). The horizontal resolution is 2 km. Radiation is parameterized using the Rapid Radiative Transfer Model for GCMs (RRTMG) (Mlawer et al. 1997). Cloud microphysics are parameterized using the SAM one-moment scheme. For the purposes of replicability and comparability, we borrowed many modeling parameters from the Radiative Convective Equilibrium Model Intercomparison Project (RCEMIP) protocol (Wing et al. 2018). The vertical grid is a modified version of the RCEMIP high-vertical-resolution grid, extended to allow for greater surface temperature. It consists of 160 levels, with a vertical resolution of 40 m at the surface, 200 m at altitudes between 3 and 25 km, and increasing to 500 m above that. The model top is at 36 km. A sponge layer occupies the upper 30% of the model domain. The model stratosphere is allowed to equilibrate without any nudging of the thermodynamic profiles. To accommodate the computational cost of exploring a wide range of modeling conditions, as well as the long equilibration times required, our standard simulations use a small, 256-km domain. To test the relevance of convective organization, we use a larger 2048-km domain. Following RCEMIP, we use an idealized equatorial ozone profile and CH_4 and N_2O concentrations of 1650 and 306 ppbv, respectively. Insolation is fixed at 409.6 W m^{-2} . Unlike the RCEMIP protocol, we set CO_2 to its preindustrial value of 280 ppmv. All other well-mixed greenhouse gases are set to zero.

The model is run over a sea surface with a prescribed temperature until the atmosphere approximately reaches radiative–convective equilibrium (RCE). RCE is an idealization of the tropical atmosphere, which states that the latent heating from convection is balanced by radiative cooling in the free troposphere. Each simulation is integrated for 500 days, except for simulations without ozone, which required 1000 days to equilibrate. The data reported are from the final 40% of the model integration. We identify cloudy grid cells as those whose condensates exceed either $1 \times 10^{-5}\text{ kg kg}^{-1}$ or 1% of the saturation specific humidity, whichever is smaller. This is consistent with the method of the RCEMIP protocol as well as SAM’s own diagnostic code. Even for small domains, SAM has a high propensity to undergo convective self-aggregation, in which convection spontaneously organizes into persistent moist and dry patches (Tompkins 2001; Bretherton et al. 2005; Held et al. 1993). The spatial scale of self-aggregation depends on surface temperature (Yang 2018b), altering the climate state in ways

TABLE 1. Summary of all idealized experiments conducted in this study. Each experiment consists of eight simulations with prescribed surface temperatures of 280, 285, 290, 295, 300, 305, 310, and 315 K. The Large-Organized experiment is conducted without homogenized radiation. The Thompson experiment uses Thompson microphysics rather than the SAM one-moment scheme. The CAM Radiation experiment is conducted using the CAM3 radiation scheme rather than RRTMG.

Expt	Domain (km)	Ozone	Insolation (W m^{-2})	CO_2 (ppm)
Standard	256	Standard	409.6	280
Standard, no CO_2	256	Standard	409.6	0
Standard, $4\times\text{CO}_2$	256	Standard	409.6	1120
No Solar	256	Standard	0	0
2xSolar	256	Standard	819.2	0
H_2O -only SW	256	Standard	409.6 (absorbed only by H_2O)	0
O_3 -only SW	256	Standard	409.6 (absorbed only by O_3)	0
O_2 -only SW	256	Standard	409.6 (absorbed only by O_2)	0
Unif- O_3	256	Uniform	409.6	280
No O_3	256	None	409.6	280
Large	2048	Standard	409.6	280
Large-Organized*	2048	Standard	409.6	280
Standard-3D	80×80	Standard	409.6	280
Thompson*	256	Standard	409.6	280
CAM Radiation*	256	Standard	409.6	280

independent of the physics at interest here. To prevent this, we horizontally homogenize radiation after computing each column, except in a set of large-domain simulations testing the importance of organization. To verify that the choice of a 2D modeling domain does not give substantially altered results, we performed 200-day 3D simulations in an $80 \text{ km} \times 80 \text{ km}$ domain with a resolution of 1 km. Due to the long equilibration times required, the 3D simulations were initialized using thermodynamic profiles from an otherwise identical 2D simulation. Since cloud microphysics are known to affect the properties of convection and convective clouds (Hu et al. 2021; Sokol and Hartmann 2022), we have performed one set of simulations with Thompson microphysics (Thompson et al. 2008). Each “experiment” in this study consists of eight simulations with prescribed sea surface temperatures from 280 to 315 K. We present fifteen experiments in total, variously adjusting the CO_2 concentration, the insolation, and the ozone profile. These experiments are summarized in Table 1.

3. Results

As the climate warms, anvil clouds rise in altitude so that their temperature increases less than the air at any given level. Figure 1a shows profiles of cloud fraction from the Standard simulations (see Table 1). The cloud fraction profile has a two-peaked structure. Following the convention of other studies (Kuang and Hartmann 2007; Wing et al. 2020), we refer to upper-tropospheric peak in cloud fraction as the anvil. The anvil migrates upward as the surface warms. Figure 1b shows cloud fraction on a temperature coordinate and normalized by dividing by its local maximum value. The anvil temperature increases with warming.

We require a precise and general definition of “anvil temperature” appropriate for the wide range of surface temperature and physics perturbations in this study. Defining anvil to

be the temperature where the cloud fraction reaches its maximum value (Kuang and Hartmann 2007; Seeley et al. 2019b; Wing et al. 2020) proved inadequate for some of our experiments. The temperature of maximum cloud fraction may shift dramatically with warming due to a modest change in cloud profile shape, rather than a meaningful change in high-cloud temperature (Fig. S1 in the online supplemental material). Using a cloud-mass-weighted temperature over the entire portion of the troposphere below a certain temperature (Zelinka and Hartmann 2010; Harrop and Hartmann 2012) is also not adequate for our experiments. Given the wide range of surface temperatures in our experiments, there is not a single temperature or pressure level consistently demarcating the “upper troposphere” from the “lower troposphere.” To avoid these shortcomings, we first identify the upper-tropospheric peak in cloud fraction. Then we calculate a cloud-mass-weighted temperature over the locations where cloud coverage of at least 80% of that maximum value:

$$T_{\text{Anv}} = \frac{\int_{p_{80\%,\uparrow}}^{p_{80\%,\downarrow}} T(p) \text{CF}(p) dp}{\int_{p_{80\%,\uparrow}}^{p_{80\%,\downarrow}} \text{CF}(p) dp}, \quad (1)$$

where T is temperature; CF is cloud fraction; and $p_{80\%,\uparrow}$ and $p_{80\%,\downarrow}$ are the highest and lowest pressure levels, respectively, where the cloud fraction is at least 80% of its maximum value. This cutoff is arbitrary choice, but in the supplemental material we show that Eq. (1) gives nearly the same temperature as a strict “peak” definition except in a few cases where the shape of the cloud profile changes abruptly with warming (Fig. S3). In those cases Eq. (1) retains monotonic behavior rather than allowing an arbitrary jump in T_{Anv} . Therefore, this method is more appropriate for this study. To reduce the imprecision introduced by a discrete model resolution, we

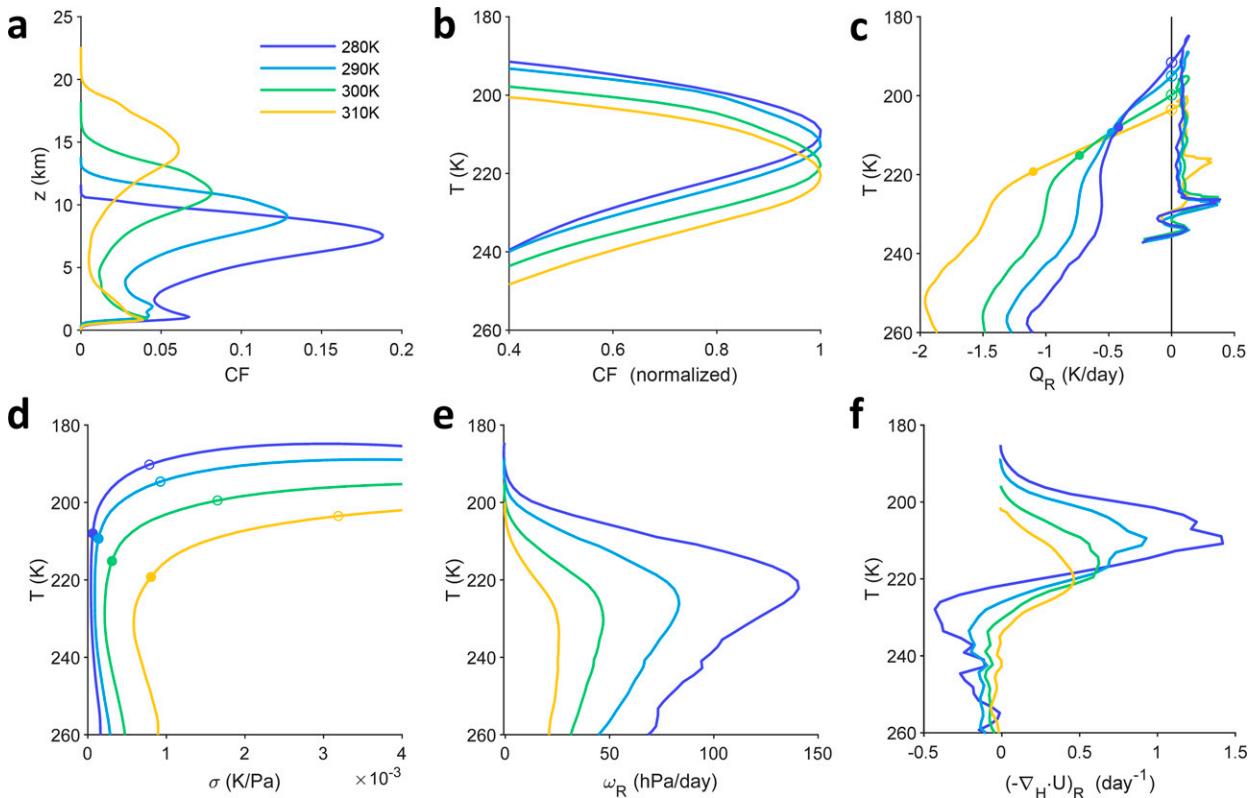


FIG. 1. The Standard experiment. (a) Profiles of cloud fraction from the Standard simulations. (b) Cloud fraction, normalized by its maximum value, and plotted against temperature. (c) All-sky radiative heating plotted against temperature. The open circles on the y intercept indicate RT. The closed circles indicate the location of T_{Conv} . (d) Static stability profiles. The open circles indicate RT. The closed circles indicate T_{Conv} . (e) Radiatively driven subsidence. (f) Radiatively driven convergence.

linearly interpolate $T(p)$ and $\text{CF}(p)$ in pressure and calculate the integral in Eq. (1) numerically.

Figure 2 shows T_{Anv} for each experiment in this study. In the Standard simulations, anvil temperature (T_{Anv}) increases by 13.2 K while the surface temperature (T_s) increases by 35 K, so that $\Delta T_{\text{Anv}}/\Delta T_s = 0.38$. The anvil warms appreciably albeit more slowly than the surface, which agrees with previous CRM and GCM studies. (Kuang and Hartmann 2007; Zelinka and Hartmann 2010; Harrop and Hartmann 2012; Khairoutdinov and Emanuel 2013). RCEMIP, whose protocol forms the basis for our experimental design, showed an average anvil warming of $\Delta T_{\text{Anv}}/\Delta T_s = 0.44$ (Wing et al. 2020).

As the climate warms, the RT becomes warmer as well. Figure 1c shows all-sky radiative heating against temperature as a vertical coordinate. Considering the troposphere as the region of the atmosphere in radiative–convective equilibrium, we identify radiative RT as the temperature at which radiative heating changes sign. That is, RT is the y intercept in Fig. 1c, marked with an open circle for each simulation. The RT temperature for the Standard experiment is shown in Fig. 2a. RT temperature (T_{RT}) increases by 14.8 K over a 35-K increase in T_s , so that $\Delta T_{\text{RT}}/\Delta T_s = 0.42$. This replicates recent studies of radiative–convective equilibrium in 1D models without clouds. Klufft et al. (2019) showed $\Delta T_{\text{RT}}/\Delta T_s \approx 0.5$ and noted that the temperature increase of

RT (or “convective top”) resembled the slow temperature increase of anvil clouds. Dacie et al. (2019) similarly showed $\Delta T_{\text{RT}}/\Delta T_s \approx 0.4$, though that study defined RT as the threshold where convective heating (or radiative cooling) equals 0.2 K day^{-1} .

a. Radiatively driven convergence

The cloud fraction profile is the result of sources and sinks of cloudy air: detrainment from the convective core and evaporation or precipitation, respectively (Seeley et al. 2019a). We focus on one component of the sources, due to the radiatively driven subsidence of air in clear skies (Kuang and Hartmann 2007; Zelinka and Hartmann 2010):

$$\omega_R = -\frac{Q_R}{\sigma}. \quad (2)$$

Here, ω_R is a pressure velocity (Pa day^{-1}), Q_R is the radiative heating rate (K day^{-1}), and σ is the static stability (K Pa^{-1}), given by

$$\sigma = \frac{\Gamma_d - \Gamma}{\rho g}, \quad (3)$$

Where Γ is the lapse rate (K m^{-1}), Γ_d is the dry-adiabatic lapse rate, ρ is density, and g is the acceleration due to gravity.

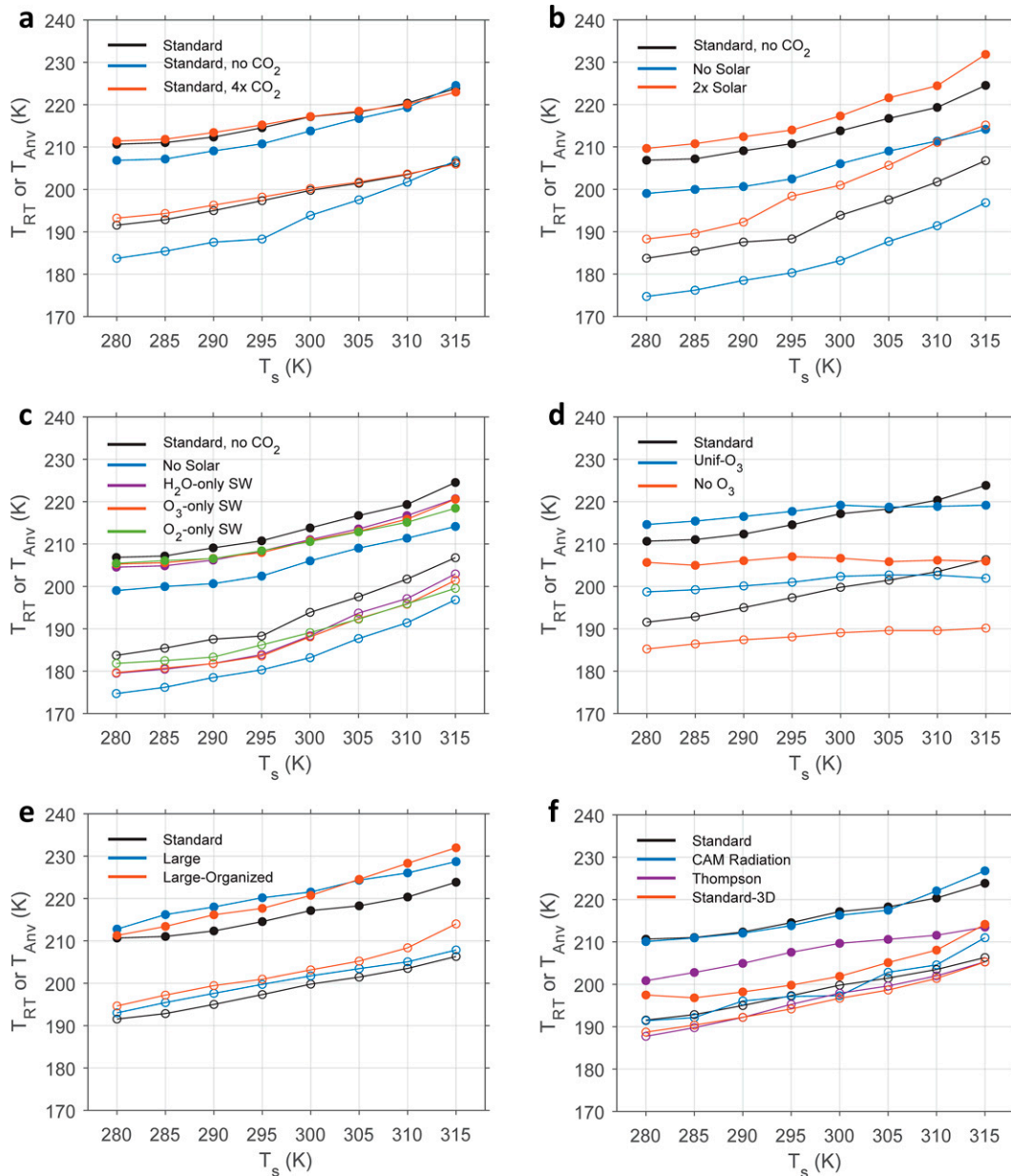


FIG. 2. RT temperature (open circles) and anvil temperature (closed circles) for each simulation used in this study. Black lines and marks indicate a simulation, also present in another panel, used as a baseline for comparison.

The radiatively driven horizontal convergence of air in clear skies is then given by:

$$(-\nabla_H \cdot \mathbf{U})_R = \partial \omega_R / \partial p. \quad (4)$$

In the absence of mean ascent or subsidence over the domain, $(-\nabla \cdot \mathbf{U})_R$ is balanced by divergence out of the convective region at the same altitude. Past modeling studies found that the peak upper-tropospheric cloud fraction tends to be located at or near the maximum in $(-\nabla_H \cdot \mathbf{U})_R$ (Kuang and Hartmann 2007; Zelinka and Hartmann 2010; Seeley et al.

2019b). \mathbf{U} is a large-scale velocity. The velocities associated with individual convective events are generally greater than \mathbf{U} but in aggregate would imply divergence from convective plumes at approximately the same level.

The radiative heating rate Q_R from the Standard experiment is shown in Fig. 1c. Since radiation is horizontally homogenized in our simulations, we use domain-averaged values of Q_R in the present calculations. Figures 1d and 1e show σ and ω_R , plotted against a temperature coordinate. The static stability σ increases with height as the atmosphere transitions from a radiative-convective equilibrium temperature profile

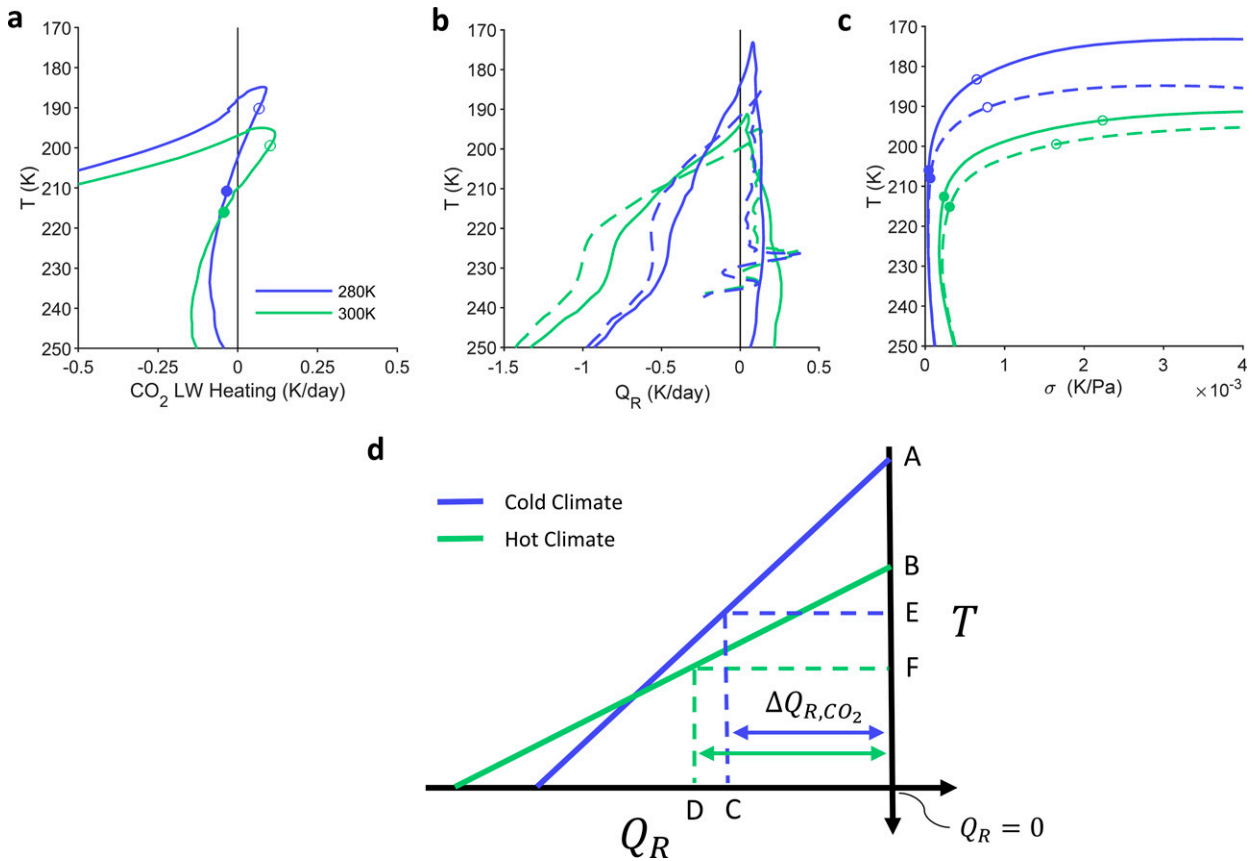


FIG. 3. The role of CO_2 . (a) The CO_2 clear-sky longwave heating rate in the Standard experiment, as obtained from offline calculations. The open circles indicate RT. The closed circles indicate T_{Conv} . (b) Radiative heating rate for the Standard experiment (dashed lines) and the Standard, no CO_2 experiment (solid lines). (c) Static stability for the Standard experiment (dashed lines) and the Standard, no CO_2 experiment (solid lines). (d) Conceptual picture of how CO_2 helps to set RT temperature. Points A and B denote the RT without CO_2 . Points C and D denote $-\Delta Q_{R,\text{CO}_2}$. Points E and F denote the RT with CO_2 .

below to a more statically stable radiative equilibrium profile above. This transition to greater static stability is coincident with a steady decline in the magnitude of Q_R toward the RT. Therefore, ω_R declines sharply with altitude at that level. The peak in radiative convergence ($-\nabla_H \cdot \mathbf{U}$) $_R$ occurs there, as shown in Fig. 1f. That peak moves to a greater temperature as the surface temperature increases, much like the peak in cloud fraction in Fig. 1b. Separately, the magnitude of ($-\nabla_H \cdot \mathbf{U}$) $_R$ declines due to increasing σ . This matches a decline in anvil cloud extent seen in Fig. 1a, consistent with the “stability iris” hypothesis described by Bony et al. (Bony et al. 2016).

b. Sensitivity to CO_2

We examine the relationship between the anvil and RT temperatures using a variety of modeling choices. We ask: do anvil temperature and RT temperature covary in response to a change of model parameters? We will focus on a sequence of experiments designed to elucidate the physical processes governing the anvil and RT. We begin by removing carbon dioxide from the Standard setup. With CO_2 removed, RT and anvil become colder. The RT temperature increases more rapidly with warming ($\Delta T_{\text{RT}}/\Delta T_s = 0.66$), as does the anvil

temperature ($\Delta T_{\text{Anv}}/\Delta T_s = 0.50$). Figure 3a shows the clear-sky CO_2 longwave heating rate from the Standard experiment. We obtain this from offline radiative transfer calculations with and without CO_2 in RRTMG, using the Standard experiment thermodynamic profiles. This calculation reasonably captures the differences in all-sky radiative heating between the Standard experiment and its no- CO_2 counterpart (Fig. 3b). In Fig. 3a, CO_2 causes net heating around RT. This may be explained by the curvature of the temperature profile: near RT CO_2 is absorbing radiation from the warm troposphere below, while only emitting at its own, relatively cold temperature (Thuburn and Craig 2002). This CO_2 heating results in a greater radiative equilibrium temperature and therefore a greater RT temperature. The anvil warming from CO_2 may be due to a shift in the static stability profile (Fig. 3c). RT marks the transition from the tropospheric RCE temperature profile below to the approximate radiative equilibrium profile above, which requires a sharp increase in static stability in the upper troposphere. Via Eqs. (2) and (4), this helps to set the peak radiatively driven convergence and anvil location, linking the RT to the anvil.

To understand the difference in RT *trend* with warming due to CO_2 , we offer a schematic explanation in Fig. 3d. The solid

lines are the longwave heating rate for an atmosphere without CO_2 in the vicinity of RT, plotted against a temperature vertical coordinate. Conceptually, we have zoomed in on the upper portion Fig. 3b. The magnitude of Q_R declines with decreasing temperature as the water vapor concentration becomes too small to efficiently cool the atmosphere, and its dependence on temperature is dominated by this mechanism (Hartmann and Larson 2002; Jeevanjee and Fueglistaler 2020). In an atmosphere without CO_2 , RT occurs at the intercept (e.g., point A). With CO_2 , RT occurs at a lower, warmer level where the water vapor cooling can offset CO_2 heating (point E). As the climate warms, there are two competing factors at play: 1) the changing slope of the $T-Q_R$ curve, and 2) the changing magnitude of CO_2 heating near RT. The slope of the $T-Q_R$ curve declines due to the greater characteristic upper-tropospheric cooling rate at warmer surface temperatures, as seen in Fig. 1c or 3c. This may be explained by pressure effects on the transmission of radiation (Hartmann et al. 2022). The declining slope reduces the CO_2 effect on RT temperature. The CO_2 heating rate near RT is increasing with climate warming, which would enhance the CO_2 effect on RT temperature (Fig. 3a). This effect partially counters that of the declining slope of the $T-Q_R$ curve. In our simulations, the declining $T-Q_R$ slope dominates, so the RT temperature increases more slowly with CO_2 than without.

c. Sensitivity to insolation

Solar radiation also has a substantial effect on anvil and RT temperatures. With CO_2 still excluded, we also remove solar radiation from the model (Fig. 2b) and find that this cools both the RT and the anvil by about 10 K in all simulations. This is easily understood as the result of a colder stratospheric radiative equilibrium temperature, as H_2O , O_3 , and O_2 are all responsible for shortwave heating there. Since RT is the intersection of the approximate radiative equilibrium profile above and the tropospheric RCE profile below, the colder radiative equilibrium temperature results in a colder RT. Figure 2b also shows that a doubling of solar radiation has an analogous warming effect on both RT and anvil. Curiously, for both No Solar and 2xSolar, the trends $\Delta T_{\text{RT}}/\Delta T_s$ and $\Delta T_{\text{Anv}}/\Delta T_s$ are not especially sensitive to solar radiation. Since ozone heating is usually considered responsible for anvil warming, it might be surprising that this PHAT behavior persists in the absence of solar radiation. However, longwave heating by ozone is about as strong as its shortwave heating in the upper troposphere and tropopause layer (Thuburn and Craig 2002), so even in the absence of shortwave radiation there remains a substantial vertical gradient in ozone heating. Figure 2c shows three additional experiments, H_2O -only SW, O_3 -only SW, and O_2 -only SW, which selectively turn off all shortwave absorption except by H_2O , O_3 , and O_2 , respectively. These show that shortwave heating from any one of these constituents alone is sufficient to produce much of the response to solar radiation.

d. Sensitivity to O_3

Our choices regarding ozone have a profound effect on the simulated trends of anvil and RT temperature. The RCEMIP

ozone profile is based on the equatorial climatology so that it increases with height in the upper troposphere and lower stratosphere. Thus, when the surface warms, the troposphere is lifted into a region of greater ozone concentration. Beginning again from the Standard setup, we now manipulate ozone. In the Unif- O_3 experiment we remove ozone's vertical structure by prescribing a vertically uniform profile of the same column mass as in the Standard experiment. Indeed, the warming of the RT as well as the anvil are greatly reduced compared to the Standard experiment, to $\Delta T_{\text{RT}}/\Delta T_s = 0.09$ and $\Delta T_{\text{Anv}}/\Delta T_s = 0.14$, respectively.

The No- O_3 experiment achieved a similar result to Unif- O_3 (Fig. 4d), as $\Delta T_{\text{RT}}/\Delta T_s = 0.14$ and $\Delta T_{\text{Anv}}/\Delta T_s = 0.00$. The small change in anvil temperature replicates the findings of Harrop and Hartmann (Harrop and Hartmann 2012) in a similar setup. Seeley et al. (Seeley et al. 2019b), in their analogous "full complexity" simulations, found a more strictly fixed RT temperature as well as a nearly fixed anvil temperature for surface temperatures greater than freezing. That study used a different model and a small 3D domain, choices which may affect the RT temperature trend. At a tropical Earth-like surface temperature of 300 K, the No- O_3 experiment shows a colder anvil and RT than the Standard experiment, whereas the Unif- O_3 experiment is a closer match since the ozone heating warms both the anvil and RT.

e. Sensitivity to organization, domain geometry, and parameterizations

Finally, we verify that our choice of a small 2D domain and lack of convective organization do not affect our earlier conclusions. Figure 2e shows the anvil and RT temperatures for the two large-domain experiments, as well as the Standard experiment. In one experiment the radiative heating is horizontally homogenized, preventing convective organization, and in the other radiation is interactive to allow organization. Compared to the standard, small-domain simulations presented in Fig. 1 and depicted by the black marks in Fig. 2e, the anvil temperature and RT temperature are both slightly warmer but display otherwise similar trends with warming. The warmer RT and anvil may be explained by the large-domain simulations having reduced upper-tropospheric relative humidity, moving the effective emission level to a lower, warmer location (Fig. S7a). This is analogous to the findings by Harrop and Hartmann (Harrop and Hartmann 2012), who found that artificially reducing the amount of upper-tropospheric water vapor passed to the radiation scheme increased anvil temperature. Convective organization does not appear to affect the anvil temperature's trend with warming, consistent with previous studies (Wing et al. 2020; Harrop and Hartmann 2012).

Figure 2f shows a series of simulations using a small 3D domain, as well as simulations using Thompson two-moment microphysics (Thompson et al. 2008). In either case, the anvil is considerably colder than in the Standard experiment, but the trend with climate warming is similar. The anvil-RT relationship remains robust. The colder anvils appear to be the result of greater upper-tropospheric humidity in those experiments, which would move the emission level to a

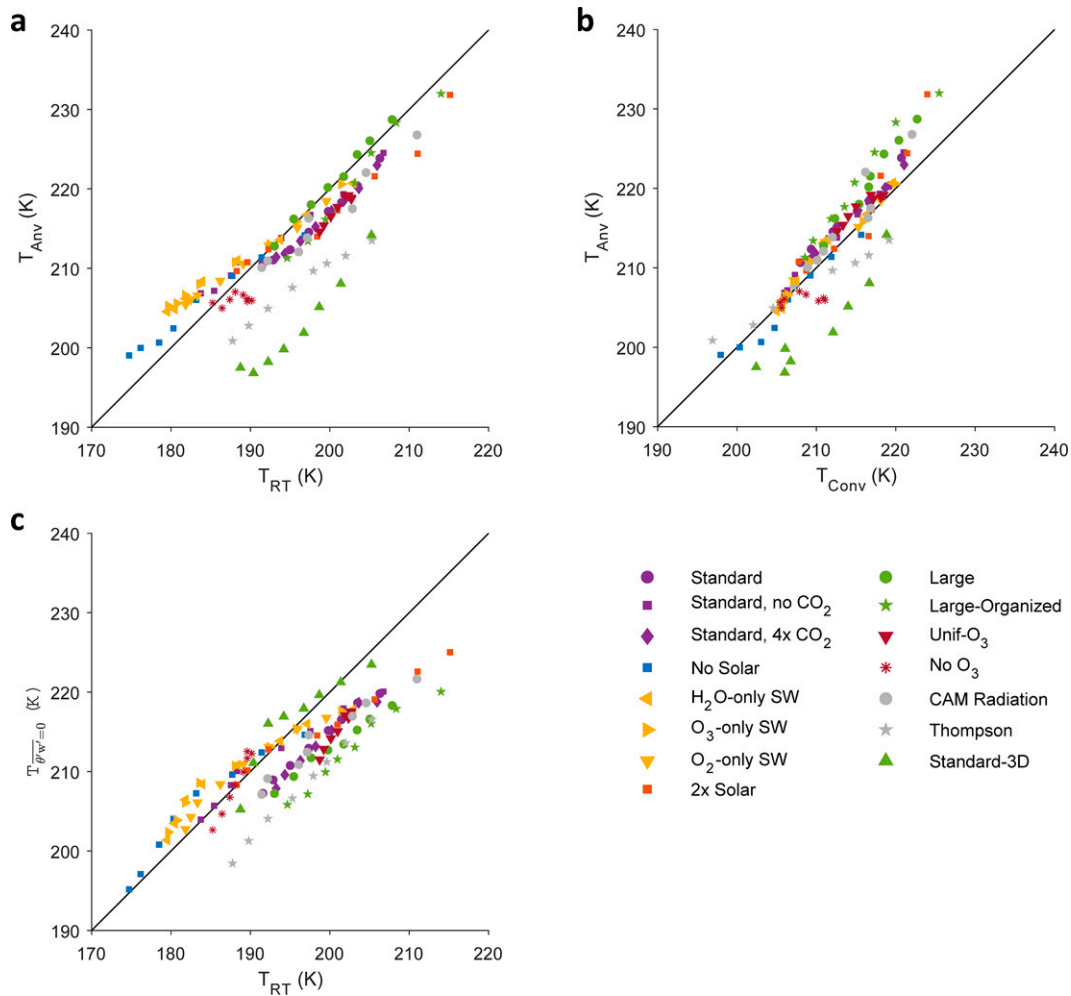


FIG. 4. Relationship between T_{RT} and T_{Anv} . (a) T_{Anv} plotted against T_{RT} for each simulation in this study. (b) T_{Anv} plotted against T_{Conv} for each simulation in this study. (c) $T_{w'\theta'_e=0}$ plotted against T_{RT} for each simulation in this study. A one-to-one line is shown in black as an aid to the reader.

colder temperature (Fig. S7b). This may arise from, or be complementary to, cloud–radiative interactions or differences between 2D and 3D convection. Another experiment using the CAM3 radiation scheme (Collins et al. 2006) demonstrates that there is only small sensitivity to our choice of radiation parameterization.

4. An anvil–radiative tropopause relationship

Throughout our experiments, we find that the temperature of the cloud anvil is empirically related to the temperature of RT. Figure 4a shows the anvil temperature plotted against the RT temperature for each simulation we conducted. Anvil and RT always occur at different locations and temperatures from one another, yet they appear closely related. If a simulation results in a warmer RT, then it generally yields a warmer anvil. This behavior appears particularly robust when comparing the temperature trends $\Delta T_{\text{trop}}/\Delta T_s$ and $\Delta T_{\text{Anv}}/\Delta T_s$ for a single experimental configuration (Fig. 5a). The anvil–RT

relationship is robust over 120 simulations in a wide range of model settings. This is our central result.

Insofar as the anvil location is set by the location of radiatively driven convergence, we would expect those locations to have similar temperatures. We define a convergence-weighted temperature similarly to how we defined an anvil temperature before:

$$T_{\text{Conv}} = \frac{\int_{p_{80\%,\uparrow}}^{p_{80\%,\downarrow}} T(p)(-\nabla_H \cdot \mathbf{U})_R dp}{\int_{p_{80\%,\uparrow}}^{p_{80\%,\downarrow}} (-\nabla_H \cdot \mathbf{U})_R dp}, \quad (5)$$

where $p_{80\%,\uparrow}$ and $p_{80\%,\downarrow}$ are the highest and lowest pressure levels where $(-\nabla_H \cdot \mathbf{U})_R$ is at least 80% of its maximum value. Figure 4b shows the relationship between this convergence-weighted temperature and anvil temperature. As found by previous studies of CRMs, GCMs, and observations, the

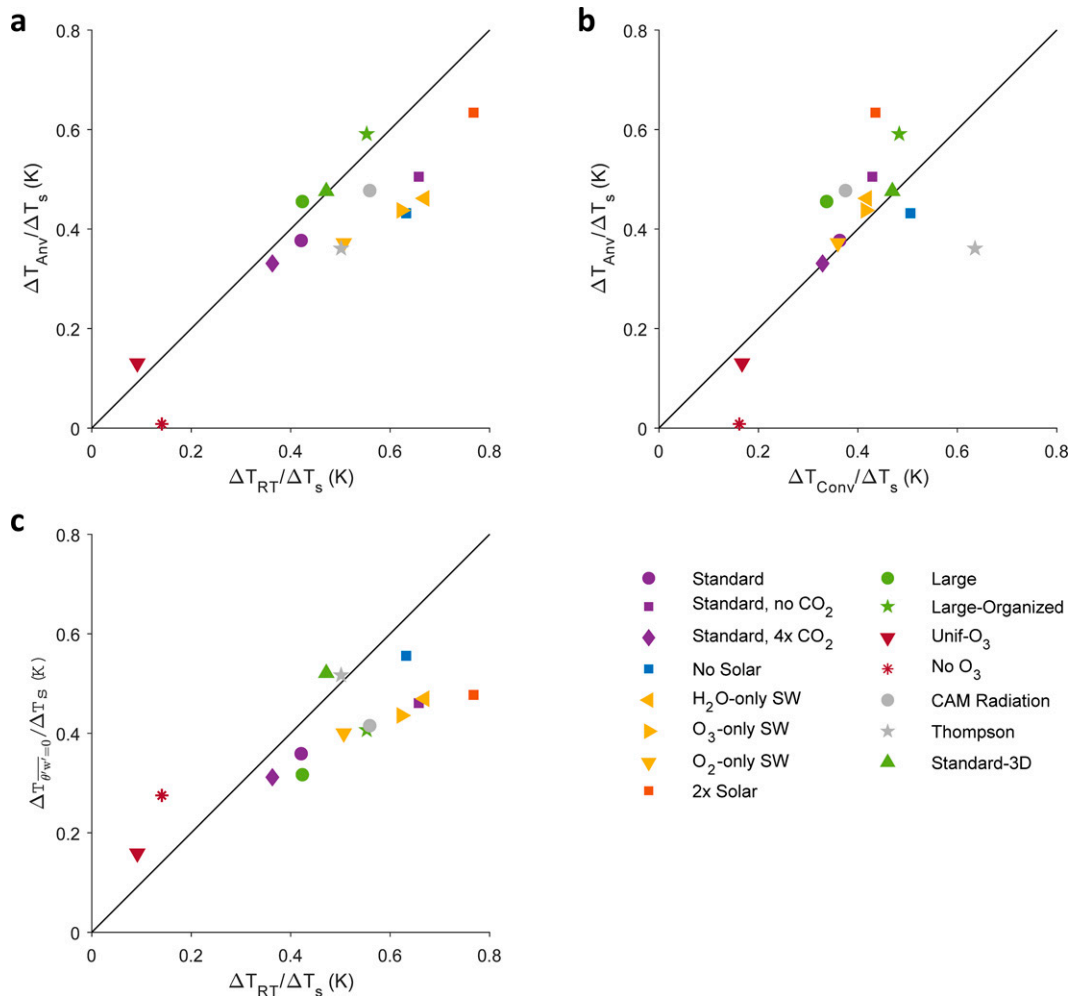


FIG. 5. Relationship between ΔT_{RT} and ΔT_{Anv} . (a) $\Delta T_{Anv}/\Delta T_s$ plotted against $\Delta T_{RT}/\Delta T_s$ for each simulation in this study. (b) $\Delta T_{Anv}/\Delta T_s$ plotted against $\Delta T_{Conv}/\Delta T_s$ for each simulation in this study. (c) $\Delta T_{\theta'w=0}/\Delta T_s$ plotted against $\Delta T_{RT}/\Delta T_s$ for each simulation in this study. A one-to-one line is shown in black as an aid to the reader.

temperature of cloud anvils is well predicted by the convergence temperature.

The empirical relationship between RT temperature, anvil temperature, and convergence temperature suggests that anvil and RT arise from related physics. If convection is comprised of a spectrum of plumes with varying entrainment rates (Arakawa and Schubert 1974), then the non-dilute (non-entraining) plume reaches the greatest altitude. The level of neutral buoyancy for the non-dilute plume occurs near RT, as convection would not be buoyant in the stable temperature profile substantially above RT. It detrains there, setting the temperature as that of the moist adiabat.

Below this level, dilute plumes are responsible for setting the temperature as colder than the moist adiabat. See, for example Figs. 1a and 2f from Zhou and Xie (Zhou and Xie 2019), which show a sharp increase in temperature relative to the moist adiabat at the top of the troposphere. This causes static stability to increase with height below RT, as seen in our Fig. 1d. The static

stability profile then links RT to the level of convergence and anvil according to Eqs. (2) and (4).

This explanation resembles that of Hartmann et al. (Hartmann et al. 2019), who noted that due to convective overshooting, the least entraining plumes inject relatively cold air above the level of the anvil (see also, Kuang and Bretherton 2004). This causes a buoyancy flux divergence which must be balanced by radiative heating, so RT appears there. Figure 6 shows a plot of virtual potential temperature flux in our Standard experiment. It is expressed as an energy flux $\rho c_p w' \theta'_v$. Above the level of zero buoyancy flux, where $w' \theta'_v = 0$, significant convective activity is present due to overshooting. RT occurs above the minimum in virtual potential temperature flux, where there is flux divergence. The temperature at the level of zero buoyancy flux is very close to T_{Conv} , indicating that convection tends to lose its buoyancy near the level of large-scale divergence from convection. The temperature at the level of zero buoyancy flux increases with surface warming at a rate comparable to both RT and anvil

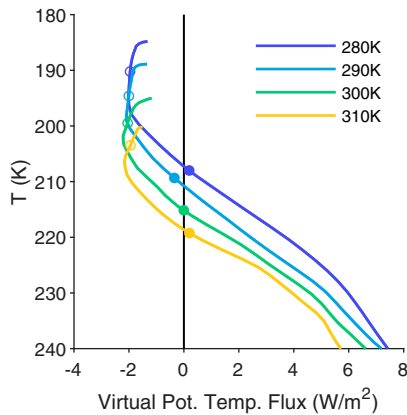


FIG. 6. Virtual potential temperature flux in the Standard experiment. The open circles indicate RT. The closed circles indicate T_{Conv} . Data are cut off at the cold point.

($\Delta T_{w' \theta' = 0} / \Delta T_s = 0.36$). Plots comparing the temperatures at the level of zero buoyancy flux and at RT across all our simulations show that they indeed covary (Figs. 4c and 5c). This corroborates the explanation provided by Hartmann et al.

However, 1D radiative–convective models simulate a similar RT temperature and trend to that found in our Standard experiment when given the same RCEMIP radiation parameters (see Kluff et al. 2019, or the “hard convective adjustment” simulations in Dacie et al. 2019). The simplest such models do not simulate or parameterize overshooting convection and its associated negative buoyancy flux, and the level of neutral buoyancy is essentially set at RT. The fact that RT is well represented in these models suggests that RT is not caused or set by the reversal in buoyancy flux. Regardless of the particular explanation, when the modeled RT and anvil each remain at a nearly fixed temperature, as in our Unif- O_3 and No- O_3 experiments, this behavior likely arises in part from the FAT mechanism. That is, the Clausius–Clapeyron scaling of saturation vapor pressure causes H_2O radiative cooling to decline near a fixed temperature (Hartmann and Larson 2002; Jeevanjee and Fueglistaler 2020).

5. Tug of war: Rising O_3 profiles versus surface warming

Our Standard simulations used an ozone profile which is fixed in pressure despite a warming surface. This is unrealistic. In the real tropical atmosphere, the ozone profile would evolve in response to deeper convective mixing of small tropospheric ozone concentrations. Additionally, upward transport of ozone may increase as stratospheric upwelling intensifies with surface warming (Lin et al. 2017). A fixed-in-pressure ozone profile will alter the equilibrium RT temperature, as ozone is the main absorber responsible for radiative heating there (Thuburn and Craig 2002). As shown in our simulations, surface warming leads to a warmer RT with a fixed O_3 profile. However, lifting the O_3 profile can lead to the local decline of ozone heating, which tends to reduce RT temperature. Therefore, there is a “tug of war” between the two effects to determine how RT temperature responds to climate warming in the

real tropical atmosphere. We cannot predict the anvil or RT temperature trend with warming using a fixed ozone profile.

To investigate the role of ozone, past studies have artificially increased upper-tropospheric ozone, leading to greater anvil temperature (Kuang and Hartmann 2007) as well as greater RT temperature (Birner and Charlesworth 2017; Dacie et al. 2019). Other authors have simply removed ozone entirely (Jeevanjee and Roms 2018; Seeley et al. 2019b; Harrop and Hartmann 2012), as in our No O_3 experiment. However, those idealized treatments of the ozone profile cannot provide a quantitative estimate of how ozone influences the warming trend of anvil or RT. Does the rising troposphere or the declining ozone concentration win the tug of war, or do they cancel one another? To answer that question, we shall prescribe ozone from the Whole Atmosphere Community Climate Model (CESM2-WACCM6), which employs coupled ozone chemistry (Gettelman et al. 2019).

We use WACCM6 data from a preindustrial control run in which the CO_2 concentration is fixed at 280 ppm (“piControl”), as well as a simulation of the response to an abrupt quadrupling of CO_2 concentration (“abrupt-4 \times CO_2 ”) (Eyring et al. 2016; Danabasoglu 2019). Those two experiments are commonly used for estimating climate feedbacks, and the large forcing results in a large difference in surface temperature. For either simulation we average the final 50 years of data, within 10° of the equator. In that region, tropical sea surface temperature increases from 301.21 K at the end of the piControl simulation to 306.65 K at the end of the abrupt-4x CO_2 simulation. Figure 7a shows that as the climate warms, the ozone concentration decreases below the 20-hPa level and increases above. Figure 7b shows that the normalized cloud profiles are nearly the same in a temperature coordinate.¹ WACCM simulates a FAT in the deep tropics. Figure 7c shows that WACCM also simulates a FiTT in the deep tropics: RT temperature increases by only 0.05 K. The coarse resolution and small surface temperature increment of the GCM output undercut the precision of this estimate, but it is nevertheless a striking result. The ozone profiles appear nearly the same in a temperature coordinate in the troposphere and tropopause layer (Fig. S8) due to nearly fixed tropospheric concentration and FiTT.

To what extent does the shifted ozone profile account for the apparent temperature-invariance of the WACCM radiative tropopause and anvil clouds? We modify our Standard formulation of 2D SAM. We conduct one simulation with the piControl surface temperature and ozone profile and a second simulation with the abrupt-4x CO_2 surface temperature and ozone profile. As a mechanism-denial experiment, we conduct a third simulation with the warmer abrupt-4x CO_2 surface temperature and the piControl ozone profile, which is shifted lower in altitude compared to the abrupt-4x CO_2 ozone profile. Consistent with the GCM simulations, we increase CO_2 by 4 times in both warming simulations.

¹ T_{Anv} as calculated from Eq. (1) decreases from 217.2 to 216.6 K. However, due to the coarseness of the GCM output, the sign and magnitude of that change depend non-monotonically on what percentage threshold we consider as the “anvil” in that formula.

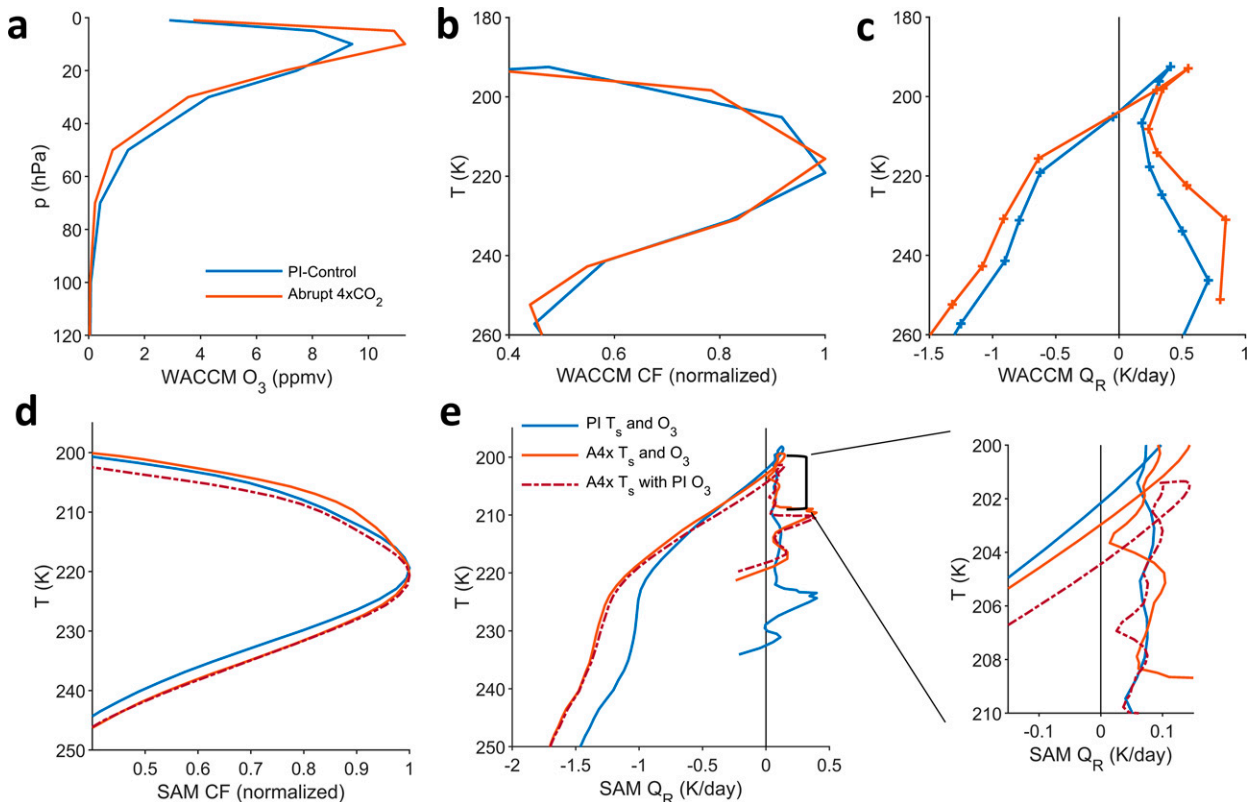


FIG. 7. CESM2-WACCM simulations and WACCM-informed SAM simulations. (a) CESM2-WACCM ozone. (b) CESM2-WACCM cloud fraction plotted against a temperature coordinate. (c) CESM2-WACCM radiative heating plotted against temperature. (d) Normalized cloud fraction for the SAM simulations based on WACCM surface temperature and ozone. (e) Radiative heating for the SAM simulations based on WACCM surface temperature and ozone.

Figure 7d shows the cloud fraction profiles of the WACCM-informed SAM simulations. With ozone prescribed to match the surface temperature, the normalized cloud fraction profile is nearly unchanged with respect to temperature. The value of T_{Anv} , calculated according to Eq. (1) increases by less than 0.1 K so that $\Delta T_{\text{Anv}}/\Delta T_s = 0.01$. When ozone is instead fixed, T_{Anv} increases by 1.3 K so that $\Delta T_{\text{Anv}}/\Delta T_s = 0.23$. The difference in T_{Anv} between the two ozone treatments is mostly attributable to greater cloud amount above the peak in the realistic-ozone scenario. The temperature at the peak itself is nearly unchanged. Figure 7e shows the radiative heating profiles of all three simulations. When ozone matches the surface temperature, T_{RT} increases by 0.8 K so that $\Delta T_{\text{RT}}/\Delta T_s = 0.15$. When ozone is instead fixed, T_{RT} increases by 2.3 K so that $\Delta T_{\text{RT}}/\Delta T_s = 0.42$. The ozone-shifted results resemble the idealized No-O₃ experiment presented earlier. For both anvil and RT, the shifted ozone profile offsets most of the warming that would occur with fixed ozone. In summary, when ozone is realistically modeled as in WACCM, the effects of increasing surface temperature and a lifted ozone profile roughly cancel one another to produce a FiTT as well as a FAT. However, the ozone we prescribe does not reflect the ozone sources and sinks associated with deep convection in SAM, but rather those of a different model. Also, our simulations are also performed without a Brewer-Dobson circulation, though Kuang and Hartmann (2007) found it had only a

small effect on anvil temperature in an idealized CRM. In future studies it may also be worthwhile to investigate more than a single GCM's representation of ozone.

The difference in anvil warming between the fixed-ozone and lifted-ozone scenarios gives rise to a difference in top-of-atmosphere radiation in SAM. The cloud-longwave radiative effect is 0.43 W m^{-2} more positive when we prescribe ozone to shift upward (or 0.31 W m^{-2} net including shortwave.) This results in a stronger positive cloud-longwave feedback by about $0.08 \text{ W m}^{-2} \text{ K}^{-1}$ (or $0.06 \text{ W m}^{-2} \text{ K}^{-1}$ net including shortwave). This is smaller than the ozone-related cloud-radiative effect of about 0.8 W m^{-2} and longwave feedback of $0.21 \text{ W m}^{-2} \text{ K}^{-1}$ found in a GCM by Nowack et al. (2015), which may be due in part to the comparatively smaller SAM cloud fraction profile.²

6. Discussion

We have shown that the temperatures of cloud anvils and radiative tropopause (RT) strongly covary across a wide range of model settings and surface temperatures in a 2D cloud-resolving

² We are comparing Nowack et al.'s B and C1 simulations. We estimated the cloud-radiative effect using the Web Plot Digitizer (Rohatgi 2019) for their Fig. 2c and a comparable 5.44 K of surface warming.

model. This affirms the intuition in FAT thinking that anvils occur near the top of the troposphere where the radiative cooling rate declines toward zero (Hartmann and Larson 2002). We have shown that the presence of CO₂ causes the anvil and RT temperatures to increase more slowly with surface warming than they otherwise would, and we have shown that solar radiation warms the RT and anvil. Both of these effects on RT temperature can be understood by considering the resulting change to the radiative equilibrium temperature there. Finally, we found that accounting for the shift in ozone profile with warming offsets the ozone-induced warming usually found in CRM studies, producing a nearly fixed RT temperature as well as a FAT.

Those results are significant in light of a recent contrary result. Seeley et al. (Seeley et al. 2019b) found that anvil temperature increased in spite of a fixed RT temperature in “minimal recipe” CRM simulations which isolated the longwave effect of water vapor from other gases present in Earth’s atmosphere. Their anvil and RT may have become decoupled because that modeling choice resulted in a greater distance between anvil and RT than would be found in more Earth-like simulations. In our Standard simulations the distance between anvil and RT is 2–3 km, substantially less than the 5–10 km reported for the minimal-recipe simulations in Seeley et al. The minimal-recipe anvil warming may be partly attributable to the exclusion of CO₂, a choice we found to increase the temperature trend with warming (Fig. 2a). The Seeley et al. “full complexity” simulations, which contain CO₂, show very little anvil warming for surface temperatures above freezing. Using the same model and a similar fixed-CO₂ setup, Romps (Romps 2020) found a near FAT for surface temperatures between 285 and 315 K. Considering the results of those studies as well as the present study, the FAT prediction appears well supported by the modeling evidence. Therefore, the contribution of Seeley et al. is principally conceptual: Although theory strongly suggests that the anvil is linked to a decline in H₂O radiative cooling at a fixed temperature (Hartmann and Larson 2002; Jeevanjee and Fueglistaler 2020), other radiatively active gases and physical processes help to shape the anvil temperature trend, or lack thereof.

Our WACCM-informed simulations showed that RT temperature is nearly fixed when the ozone profile is lifted with climate warming to match the surface temperature. In the CMIP6 piControl and abrupt-4xCO₂ experiments, used to estimate climate feedbacks and climate sensitivity, models without interactive ozone chemistry instead fix ozone at its preindustrial concentrations (Eyring et al. 2016). For those models, our results suggests their RT and anvil may be biased toward warming. This would introduce a negative bias in cloud–longwave feedback, similar to that found by Nowack et al. (Nowack et al. 2015, 2018b). Models’ representation of clouds may be improved if ozone is parameterized to respond to the rising tropopause with climate change, as suggested in recent literature (Nowack et al. 2018a; Hardiman et al. 2019; Meraner et al. 2020). The continued development of models with interactive ozone chemistry, such as those documented by the Chemistry–Climate Model Initiative (CCMI), may also improve the simulation of clouds (Morgenstern et al. 2017).

Finally, we mention several caveats to this study. To afford the computational expense of conducting 123 500-day simulations,

we use a small, two-dimensional domain. We prescribe no mean ascent or descent, whereas real tropical anvil clouds form in the context of mean ascent in both the troposphere and the stratosphere. We homogenize the radiation in all our experiments except for one, which may decouple any cloud–radiation feedback. Our analysis relates cloud amount to the radiatively driven convergence in clear skies. However, that is not a closed budget for cloud amount. Other factors are known to cause detrainment from the convective core, and cloud lifetime after detrainment depends on evaporation, microphysics, and within-cloud turbulence (Lilly 1988; Hartmann et al. 2018; Gasparini et al. 2019; Seeley et al. 2019a). The peak cloud amount itself also depends on microphysics as well as model resolution (Sokol and Hartmann 2022; Jeevanjee and Zhou 2022), and there is more work to be done to understand how cloud properties depend on these choices. As with other studies on this topic, we only consider the temperature of the cloud near its peak amount, not its effective radiating temperature, which may be different.

Acknowledgments. This work was supported by a Packard Fellowship for Science and Engineering, and the France-Berkeley Fund. We acknowledge the World Climate Research Programme and its Working Group on Coupled Modelling, which coordinated and promoted CMIP6. We thank the Earth System Grid Federation (ESGF) for archiving the data and providing access, and the multiple funding agencies who support CMIP6 and ESGF. Computational resources were provided by the Department of Energy’s National Energy Research Scientific Computing Center (NERSC). SAM was provided by M. Khairoutdinov (<http://rossby.msrc.sunysb.edu/~marat/SAM.html>). The authors thank Thomas Birner, Dennis Hartmann, and one anonymous reviewer for their helpful comments and suggestions.

Data availability statement. Model output used to achieve these results can be found at the UC Davis Box website: <https://ucdavis.box.com/s/s7fbvld2rt2bfns5vof97wrbcvgc38hgm>. Additional data related to this paper may be requested from the authors.

REFERENCES

- Arakawa, A., and W. H. Schubert, 1974: Interaction of a cumulus cloud ensemble with the large-scale environment, part I. *J. Atmos. Sci.*, **31**, 674–701, [https://doi.org/10.1175/1520-0469\(1974\)031<0674:IOACCE>2.0.CO;2](https://doi.org/10.1175/1520-0469(1974)031<0674:IOACCE>2.0.CO;2).
- Birner, T., and E. J. Charlesworth, 2017: On the relative importance of radiative and dynamical heating for tropical tropopause temperatures. *J. Geophys. Res. Atmos.*, **122**, 6782–6797, <https://doi.org/10.1002/2016JD026445>.
- Blossey, P. N., Z. Kuang, and D. M. Romps, 2010: Isotopic composition of water in the tropical tropopause layer in cloud-resolving simulations of an idealized tropical circulation. *J. Geophys. Res.*, **115**, D24309, <https://doi.org/10.1029/2010JD014554>.
- Bony, S., B. Stevens, D. Coppin, T. Becker, K. A. Reed, A. Voigt, and B. Medeiros, 2016: Thermodynamic control of anvil cloud amount. *Proc. Natl. Acad. Sci. USA*, **113**, 8927–8932, <https://doi.org/10.1073/pnas.1601472113>.
- Bretherton, C. S., P. N. Blossey, and M. Khairoutdinov, 2005: An energy-balance analysis of deep convective self-aggregation

- above uniform SST. *J. Atmos. Sci.*, **62**, 4273–4292, <https://doi.org/10.1175/JAS3614.1>.
- Collins, W. D., and Coauthors, 2006: The formulation and atmospheric simulation of the Community Atmosphere Model version 3 (CAM3). *J. Climate*, **19**, 2144–2161, <https://doi.org/10.1175/JCLI3760.1>.
- Dacie, S., and Coauthors, 2019: A 1D RCE study of factors affecting the tropical tropopause layer and surface climate. *J. Climate*, **32**, 6769–6782, <https://doi.org/10.1175/JCLI-D-18-0778.1>.
- Danabasoglu, G., 2019: NCAR CESM2-WACCM model output prepared for CMIP6 CMIP (version 20190730). Earth System Grid Federation, accessed 20 September 2021, <https://doi.org/10.22033/ESGF/CMIP6.10024>.
- Eyring, V., S. Bony, G. A. Meehl, C. A. Senior, B. Stevens, R. J. Stouffer, and K. E. Taylor, 2016: Overview of the Coupled Model Intercomparison Project Phase 6 (CMIP6) experimental design and organization. *Geosci. Model Dev.*, **9**, 1937–1958, <https://doi.org/10.5194/gmd-9-1937-2016>.
- Forster, P. M., and Coauthors, 2021: The Earth’s energy budget, climate feedbacks, and climate sensitivity. *Climate Change 2021: The Physical Science Basis*, V. Masson-Delmotte et al., Eds., Cambridge University Press, 923–1054.
- Gasparini, B., P. N. Blossey, D. L. Hartmann, G. Lin, and J. Fan, 2019: What drives the life cycle of tropical anvil clouds? *J. Adv. Model. Earth Syst.*, **11**, 2586–2605, <https://doi.org/10.1029/2019MS001736>.
- Gottelman, A., and Coauthors, 2019: The Whole Atmosphere Community Climate Model Version 6 (WACCM6). *J. Geophys. Res. Atmos.*, **124**, 12 380–12 403, <https://doi.org/10.1029/2019JD030943>.
- Grabowski, W. W., J. I. Yano, and M. W. Moncrieff, 2000: Cloud resolving modeling of tropical circulations driven by large-scale SST gradients. *J. Atmos. Sci.*, **57**, 2022–2040, [https://doi.org/10.1175/1520-0469\(2000\)057<2022:CRMOTC>2.0.CO;2](https://doi.org/10.1175/1520-0469(2000)057<2022:CRMOTC>2.0.CO;2).
- Hardiman, S. C., and Coauthors, 2019: The impact of prescribed ozone in climate projections run with HadGEM3-GC3.1. *J. Adv. Model. Earth Syst.*, **11**, 3443–3453, <https://doi.org/10.1029/2019MS001714>.
- Harrop, B. E., and D. L. Hartmann, 2012: Testing the role of radiation in determining tropical cloud-top temperature. *J. Climate*, **25**, 5731–5747, <https://doi.org/10.1175/JCLI-D-11-00445.1>.
- Hartmann, D. L., and K. Larson, 2002: An important constraint on tropical cloud-climate feedback. *Geophys. Res. Lett.*, **29**, 1195, <https://doi.org/10.1029/2002GL015835>.
- , B. Gasparini, S. E. Berry, and P. N. Blossey, 2018: The life cycle and net radiative effect of tropical anvil clouds. *J. Adv. Model. Earth Syst.*, **10**, 3012–3029, <https://doi.org/10.1029/2018MS001484>.
- , P. N. Blossey, and B. D. Dygert, 2019: Convection and climate: What have we learned from simple models and simplified settings? *Curr. Climate Change Rep.*, **5**, 196–206, <https://doi.org/10.1007/s40641-019-00136-9>.
- , B. D. Dygert, P. N. Blossey, Q. Fu, and A. B. Sokol, 2022: The vertical profile of radiative cooling and lapse rate in a warming climate. *J. Climate*, **35**, 2653–2665, <https://doi.org/10.1175/JCLI-D-21-0861.1>.
- Held, I. M., R. S. Hemler, and V. Ramaswamy, 1993: Radiative-convective equilibrium with explicit two-dimensional moist convection. *J. Atmos. Sci.*, **50**, 3909–3927, [https://doi.org/10.1175/1520-0469\(1993\)050<3909:RCEWET>2.0.CO;2](https://doi.org/10.1175/1520-0469(1993)050<3909:RCEWET>2.0.CO;2).
- Hu, S., and G. K. Vallis, 2019: Meridional structure and future changes of tropopause height and temperature. *Quart. J. Roy. Meteor. Soc.*, **145**, 2698–2717, <https://doi.org/10.1002/qj.3587>.
- Hu, Z., F. Lamraoui, and Z. Kuang, 2021: Influence of upper-troposphere stratification and cloud–radiation interaction on convective overshoots in the tropical tropopause layer. *J. Atmos. Sci.*, **78**, 2493–2509, <https://doi.org/10.1175/JAS-D-20-0241.1>.
- Jeevanjee, N., and D. M. Romps, 2018: Mean precipitation change from a deepening troposphere. *Proc. Natl. Acad. Sci. USA*, **115**, 11 465–11 470, <https://doi.org/10.1073/pnas.1720683115>.
- , and S. Fueglistaler, 2020: Simple spectral models for atmospheric radiative cooling. *J. Atmos. Sci.*, **77**, 479–497, <https://doi.org/10.1175/JAS-D-18-0347.1>.
- , and L. Zhou, 2022: On the resolution-dependence of anvil cloud fraction and precipitation efficiency in radiative-convective equilibrium. *J. Adv. Model. Earth Syst.*, **14**, e2021MS002759, <https://doi.org/10.1029/2021MS002759>.
- Khairoutdinov, M., and D. A. Randall, 2003: Cloud resolving modeling of the ARM summer 1997 IOP: Model formulation, results, uncertainties, and sensitivities. *J. Atmos. Sci.*, **60**, 607–625, [https://doi.org/10.1175/1520-0469\(2003\)060<0607:CRMOTA>2.0.CO;2](https://doi.org/10.1175/1520-0469(2003)060<0607:CRMOTA>2.0.CO;2).
- , and K. Emanuel, 2013: Rotating radiative-convective equilibrium simulated by a cloud-resolving model. *J. Adv. Model. Earth Syst.*, **5**, 816–825, <https://doi.org/10.1002/2013MS000253>.
- Kluft, L., S. Dacie, S. A. Buehler, H. Schmidt, and B. Stevens, 2019: Re-examining the first climate models: Climate sensitivity of a modern radiative-convective equilibrium model. *J. Climate*, **32**, 8111–8125, <https://doi.org/10.1175/JCLI-D-18-0774.1>.
- Kuang, Z., and C. S. Bretherton, 2004: Convective influence on the heat balance of the tropical tropopause layer: A cloud-resolving model study. *J. Atmos. Sci.*, **61**, 2919–2927, <https://doi.org/10.1175/JAS-3306.1>.
- , and D. L. Hartmann, 2007: Testing the fixed anvil temperature hypothesis in a cloud-resolving model. *J. Climate*, **20**, 2051–2057, <https://doi.org/10.1175/JCLI4124.1>.
- Lilly, D. K., 1988: Cirrus outflow dynamics. *J. Atmos. Sci.*, **45**, 1594–1605, [https://doi.org/10.1175/1520-0469\(1988\)045<1594:COD>2.0.CO;2](https://doi.org/10.1175/1520-0469(1988)045<1594:COD>2.0.CO;2).
- Lin, P., D. Paynter, Y. Ming, and V. Ramaswamy, 2017: Changes of the tropical tropopause layer under global warming. *J. Climate*, **30**, 1245–1258, <https://doi.org/10.1175/JCLI-D-16-0457.1>.
- Meraner, K., S. Rast, and H. Schmidt, 2020: How useful is a linear ozone parameterization for global climate modeling? *J. Adv. Model. Earth Syst.*, **12**, e2019MS002003, <https://doi.org/10.1029/2019MS002003>.
- Mlawer, E. J., S. J. Taubman, P. D. Brown, M. J. Iacono, and S. A. Clough, 1997: Radiative transfer for inhomogeneous atmospheres: RRTM, a validated correlated-k model for the longwave. *J. Geophys. Res.*, **102**, 16 663–16 682, <https://doi.org/10.1029/97JD00237>.
- Morgenstern, O., and Coauthors, 2017: Review of the global models used within phase 1 of the Chemistry–Climate Model Initiative (CCMI). *Geosci. Model Dev.*, **10**, 639–671, <https://doi.org/10.5194/gmd-10-639-2017>.
- Narenpitak, P., C. S. Bretherton, and M. F. Khairoutdinov, 2017: Cloud and circulation feedbacks in a near-global aquaplanet cloud-resolving model. *J. Adv. Model. Earth Syst.*, **9**, 1069–1090, <https://doi.org/10.1002/2016MS000872>.
- Nowack, P. J., N. Luke Abraham, A. C. Maycock, P. Braesicke, J. M. Gregory, M. M. Joshi, A. Osprey, and J. A. Pyle, 2015: A large ozone-circulation feedback and its implications for global warming assessments. *Nat. Climate Change*, **5**, 41–45, <https://doi.org/10.1038/nclimate2451>.
- , P. Braesicke, J. Haigh, N. L. Abraham, J. Pyle, and A. Voulgarakis, 2018a: Using machine learning to build

- temperature-based ozone parameterizations for climate sensitivity simulations. *Environ. Res. Lett.*, **13**, 104016, <https://doi.org/10.1088/1748-9326/aae2be>.
- , N. L. Abraham, P. Braesicke, and J. A. Pyle, 2018b: The impact of stratospheric ozone feedbacks on climate sensitivity estimates. *J. Geophys. Res. Atmos.*, **123**, 4630–4641, <https://doi.org/10.1002/2017JD027943>.
- Rohatgi, A., 2019: WebPlotDigitizer. Accessed 30 May 2022, <https://automeris.io/WebPlotDigitizer/>.
- Romps, D. M., 2020: Climate sensitivity and the direct effect of carbon dioxide in a limited-area cloud-resolving model. *J. Climate*, **33**, 3413–3429, <https://doi.org/10.1175/JCLI-D-19-0682.1>.
- Seeley, J. T., N. Jeevanjee, W. Langhans, and D. M. Romps, 2019a: Formation of tropical anvil clouds by slow evaporation. *Geophys. Res. Lett.*, **46**, 492–501, <https://doi.org/10.1029/2018GL080747>.
- , —, and D. M. Romps, 2019b: FAT or FiTT: Are anvil clouds or the tropopause temperature invariant? *Geophys. Res. Lett.*, **46**, 1842–1850, <https://doi.org/10.1029/2018GL080096>.
- Seidel, S. D., and D. Yang, 2020: The lightness of water vapor helps to stabilize tropical climate. *Sci. Adv.*, **6**, eaba1951, <https://doi.org/10.1126/sciadv.aba1951>.
- Sokol, A. B., and D. L. Hartmann, 2022: Radiative cooling, latent heating, and cloud ice in the tropical upper troposphere. *J. Climate*, **35**, 1643–1654, <https://doi.org/10.1175/JCLI-D-21-0444.1>.
- Thompson, D. W. J., S. Bony, and Y. Li, 2017: Thermodynamic constraint on the depth of the global tropospheric circulation. *Proc. Natl. Acad. Sci. USA*, **114**, 8181–8186, <https://doi.org/10.1073/pnas.1620493114>.
- Thompson, G., P. R. Field, R. M. Rasmussen, and W. D. Hall, 2008: Explicit forecasts of winter precipitation using an improved bulk microphysics scheme. Part II: Implementation of a new snow parameterization. *Mon. Wea. Rev.*, **136**, 5095–5115, <https://doi.org/10.1175/2008MWR2387.1>.
- Thuburn, J., and G. C. Craig, 2002: On the temperature structure of the tropical stratosphere. *J. Geophys. Res.*, **107**, 4017, <https://doi.org/10.1029/2001JD000448>.
- Tompkins, A. M., 2001: Organization of tropical convection in low vertical wind shears: The role of water vapor. *J. Atmos. Sci.*, **58**, 529–545, [https://doi.org/10.1175/1520-0469\(2001\)058<0529:OOTCIL>2.0.CO;2](https://doi.org/10.1175/1520-0469(2001)058<0529:OOTCIL>2.0.CO;2).
- , and G. C. Craig, 1999: Sensitivity of tropical convection to sea surface temperature in the absence of large-scale flow. *J. Climate*, **12**, 462–476, [https://doi.org/10.1175/1520-0442\(1999\)012<0462:SOTCTS>2.0.CO;2](https://doi.org/10.1175/1520-0442(1999)012<0462:SOTCTS>2.0.CO;2).
- Vallis, G. K., P. Zurita-Gotor, C. Cairns, and J. Kidston, 2015: Response of the large-scale structure of the atmosphere to global warming. *Quart. J. Roy. Meteor. Soc.*, **141**, 1479–1501, <https://doi.org/10.1002/qj.2456>.
- Wing, A. A., K. A. Reed, M. Satoh, B. Stevens, S. Bony, and T. Ohno, 2018: Radiative-convective equilibrium model inter-comparison project. *Geosci. Model Dev.*, **11**, 793–813, <https://doi.org/10.5194/gmd-11-793-2018>.
- , and Coauthors, 2020: Clouds and convective self-aggregation in a multimodel ensemble of radiative-convective equilibrium simulations. *J. Adv. Model. Earth Syst.*, **12**, e2020MS002138, <https://doi.org/10.1029/2020MS002138>.
- Yang, D., 2018a: Boundary layer diabatic processes, the virtual effect, and convective self-aggregation. *J. Adv. Model. Earth Syst.*, **10**, 2163–2176, <https://doi.org/10.1029/2017MS001261>.
- , 2018b: Boundary layer height and buoyancy determine the horizontal scale of convective self-aggregation. *J. Atmos. Sci.*, **75**, 469–478, <https://doi.org/10.1175/JAS-D-17-0150.1>.
- Zelinka, M. D., and D. L. Hartmann, 2010: Why is longwave cloud feedback positive? *J. Geophys. Res.*, **115**, D16117, <https://doi.org/10.1029/2010JD013817>.
- , and —, 2011: The observed sensitivity of high clouds to mean surface temperature anomalies in the tropics. *J. Geophys. Res.*, **116**, D23103, <https://doi.org/10.1029/2011JD016459>.
- Zhou, W., and S. P. Xie, 2019: A conceptual spectral plume model for understanding tropical temperature profile and convective updraft velocities. *J. Atmos. Sci.*, **76**, 2801–2814, <https://doi.org/10.1175/JAS-D-18-0330.1>.